AIP | Applied Physics Letters

Si 3 N 4 optomechanical crystals in the resolved-sideband regime

M. Davanço, S. Ates, Y. Liu, and K. Srinivasan

Citation: Applied Physics Letters **104**, 041101 (2014); doi: 10.1063/1.4858975
View online: http://dx.doi.org/10.1063/1.4858975
View Table of Contents: http://scitation.aip.org/content/aip/journal/apl/104/4?ver=pdfcov
Published by the AIP Publishing

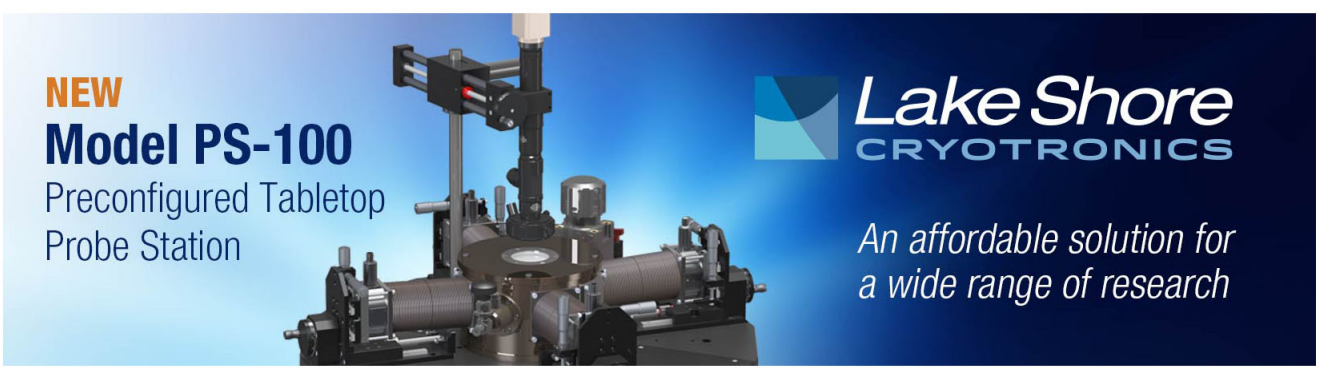

This article is copyrighted as indicated in the article. Reuse of AIP content is subject to the terms at: http://scitation.aip.org/termsconditions. Downloaded to IP: 131.215.71.79 On: Thu, 20 Mar 2014 14:54:09

Si_3N_4 optomechanical crystals in the resolved-sideband regime

M. Davanço,[1,2,a)] S. Ates,[1,3,b)] Y. Liu,[1,3,c)] and K. Srinivasan[1]
[1]*Center for Nanoscale Science and Technology, National Institute of Standards and Technology, Gaithersburg, Maryland 20899, USA*
[2]*Department of Applied Physics, California Institute of Technology, Pasadena, California 91125, USA*
[3]*Maryland NanoCenter, University of Maryland, College Park, Maryland 20742, USA*

(Received 21 November 2013; accepted 13 December 2013; published online 27 January 2014)

We demonstrate sideband-resolved Si_3N_4 optomechanical crystals supporting 10^5 quality factor optical modes at 980 nm, coupled to ≈4 GHz frequency mechanical modes with quality factors of ≈3000. Optomechanical electromagnetically induced transparency and absorption are observed at room temperature and in atmosphere with intracavity photon numbers in excess of 10^4. © *2014 AIP Publishing LLC*. [http://dx.doi.org/10.1063/1.4858975]

Silicon optomechanical crystals (OMCs) have been used to demonstrate important steps on the road to performing chip-scale quantum mechanical operations with individual phonons of a mesoscopic object. In Ref. 1, coherent interaction between cavity photons and phonons was used to demonstrate electromagnetically induced transparency (EIT) mediated by a mechanical resonance; radiation-pressure cooling of one OMC mechanical resonance to its ground state was shown in Ref. 2. Silicon OMCs are characterized by several properties that have enabled these demonstrations. They support co-localized GHz mechanical and near-infrared optical resonances that interact via radiation pressure, with large zero-point optomechanical coupling rates (g_0) between cavity photons and phonons. High quality factor ($Q_o > 10^6$) optical resonances can be achieved, with linewidth κ smaller than the few-GHz mechanical resonance frequency f_m. This places the system in the resolved-sideband regime ($\omega_m/\kappa > 1$, $\omega_m = 2\pi f_m$), in which efficient radiation-pressure dynamical back-action effects can be observed.[3] Lastly, mechanical resonances with high quality factors ($Q_m > 10^5$) are achievable, necessary for pronounced optomechanical interactions, as quantified by the cooperativity parameter $C = 4Ng_0^2/\kappa\gamma_i$ (N is the intracavity photon number and γ_i is the mechanical linewidth). Large C is necessary for effective laser cooling[2,3] and coherent photon-phonon exchange[4,5] and is achieved in Si OMCs due to their aforementioned small γ_i, small κ, and large g_0. C also scales linearly with the intracavity photon population, and thus large N provides another route to appreciable C, as observed in systems such as silica microtoroids[5] and superconducting cavity electromechanical circuits.[6] This strategy has found limited use in Si OMCs because of silicon's large two-photon absorption coefficient, which leads to reduced Q_o for large N.

As an alternative to Si, Si_3N_4 is a potentially advantageous material for OMCs: it does not exhibit two-photon absorption at relevant wavelengths; like Si, it lends itself to chip-scale nanofabrication with mature techniques; stoichiometric Si_3N_4 films under tensile stress have been shown to support high optical and mechanical Qs (≈10^6 (Refs. 7 and 8)); and Si_3N_4 is transparent over the visible and near-infrared bands, contrasting with Si, which is opaque below 1 μm. The latter is crucial for interaction with a variety of quantum optical systems that operate at shorter wavelengths, such as semiconductor quantum dots, single molecules in organic crystals, nitrogen-vacancy defects in diamond, and trapped atoms and ions.

Here, we design and experimentally investigate Si_3N_4-based OMCs in the resolved-sideband limit for light in the 980 nm wavelength range. The sideband resolution achieved was sufficient for observing, at room temperature and atmospheric pressure, EIT mediated by a ≈4 GHz mechanical mode. Our OMC consists of a suspended Si_3N_4 nanobeam of thickness $t = 350$ nm and width $w = 760$ nm, with an etched array of elliptical holes as shown in Fig. 1(a). In the outer mirror sections, the spacing a between the holes is constant while within the cavity section, it varies quadratically from the center outwards. The cavity section forms a defect in an otherwise perfect 1D photonic bandgap structure. The lattice modulation is designed to support localized, high Q ($Q_o > 10^6$) transverse-electric (TE, with $\mathbf{E_z} = 0$ on the xy plane) optical modes in the 980 nm band, co-located with breathing-type mechanical resonances at $f_m \approx 4$ GHz (respectively, shown in Figs. 1(b) and 1(c)). Figure 1(d) shows a scanning electron microscope (SEM) image of a nanofabricated device, where it is clear that in addition to the lattice spacing modulation, the aspect ratio of the holes is adjusted from the cavity region outwards. As detailed below, the design procedure leading to this final geometry involved finite-element method determination of optical and mechanical resonances and the optomechanical coupling rate g_0 due to radiation-pressure. The latter was calculated from modal electromagnetic field and mechanical displacement profiles via a first-order perturbative expression described in the supplementary material,[9] which only takes into account the moving-boundary contribution to the optomechanical coupling. Contributions from stress-induced changes of the refractive index (photoelastic effect) were not considered although they may be significant, as those in crystalline silicon nanostructures.[10,11]

[a)]mdavanco@nist.gov
[b)]Current address: The National Research Institute of Electronics and Cryptology, The Scientific and Technological Research Council of Turkey, Gebze 41400, Turkey.
[c)]Current address: Department of Mechanical Engineering, Worcester Polytechnic Institute, 100 Institute Road, Worcester, Massachusetts 01609-2280, USA.

 © 2014 AIP Publishing LLC

This article is copyrighted as indicated in the article. Reuse of AIP content is subject to the terms at: http://scitation.aip.org/termsconditions. Downloaded to IP: 131.215.71.79 On: Thu, 20 Mar 2014 14:54:09

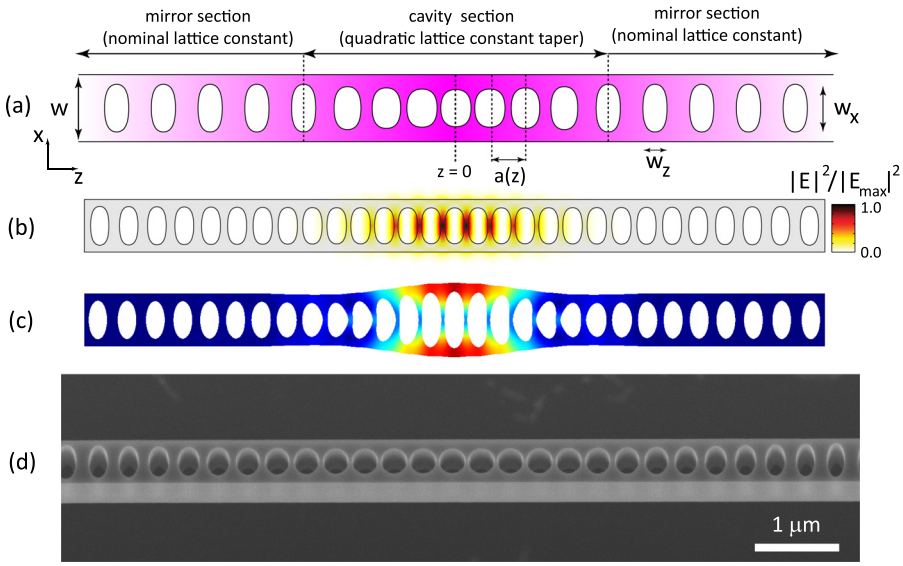

FIG. 1. (a) Optomechanical crystal geometry. (b) First-order optical resonance. (c) First-order breathing mechanical mode. (d) SEM of fabricated OMC.

We next detail our design procedure. TE photonic bands for a 1D nanobeam photonic crystal are shown in Fig. 2(a). Modes on the dielectric and air bands are of fist order in the transverse (x) direction (black lines correspond to higher transversal order modes). Parameters for the cavity section of the OMC (see Fig. 1(a)) were obtained iteratively as follows. For fixed thickness $t = 350$ nm and aspect ratio w_z/w_x, and an initial guess for the width w, a lattice constant a was selected such that the edge of the dielectric band at the **X** point ($k_z = \pi/a$) fell close to the desired resonance wavelength. The width w was varied, the **X**-point dielectric band edge was recalculated, the lattice constant a was adjusted, and the procedure was repeated until convergence of the dielectric band edge to the desired wavelength was reached. Once the lattice constant for the cavity section was determined, the effect of varying this parameter along the OMC (in the $z-$direction) was evaluated. As shown in Fig. 2(b), increasing the lattice constant along z while keeping all other dimensions fixed causes the dielectric band edge to red-shift, creating the condition for optical confinement by the photonic bandgap: the lattice constant is increased quadratically from the cavity center ($z = 0$) towards the edges so that the allowed frequency at $z = 0$ (dashed line) falls within the bandgap of the outer regions (e.g., $z = 5\,\mu$m). The cavity can also be regarded as a distributed reflector with a locally varying, distributed reflectivity as in the bottom panel in Fig. 2(b), which is close to linear near $z = 0$. Linear mirror strength profiles[9] tend to produce optical modes with reduced spatial harmonics above the light line. This leads to reduced power leakage into the air, and thus higher optical quality factors.[12,13] Confined modes with optical quality factors in excess of 10^6 were obtained simply with the lattice profile of Fig. 2(b) and $w_z/w_x \approx 0.5$. We note that because Si_3N_4 has a considerably smaller refractive index than Si (2.0 in contrast with 3.5), the achievable local reflectivities are correspondingly smaller, and thus in general the number of unit cells necessary for a high Q_o cavity is larger, and so are the obtained mode volumes.

The resulting 1D photonic crystal geometries support a phononic bandgap that is used to generate a localized mechanical mode. The mechanical bands for the crystal with photonic bands shown in Fig. 2(a) are plotted in Fig. 3(a), for a lattice constant $a = 350$ nm. Thick lines indicate spatially symmetric displacement across the x-z and y-z-planes, gray lines to other symmetries. A phononic bandgap exists between the A and B bands (shaded region). Near the Γ-point, modes on the band B (red line) have a displacement pattern that gives rise to breathing resonances where the outer nanobeam walls expand or

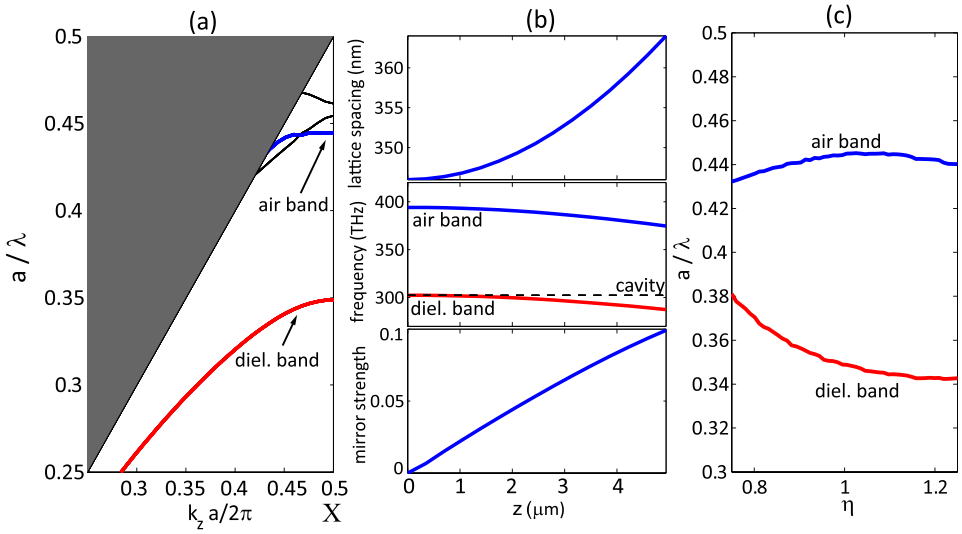

FIG. 2. (a) TE-polarization photonic bands for a periodic array of holes. Dielectric and air band modes are of first order in the x direction. Black curves: high order modes. (b) Hole spacing (top), **X**-point dielectric and air band frequencies (middle) and effective mirror strength (bottom) as functions of distance z along the cavity ($z = 0$ is the cavity center) for a high Q_o OMC cavity. (c) Evolution of the **X**-point dielectric and air band frequencies as a function of the hole aspect ratio factor $\eta = \sqrt{w_x/w_z}$.

This article is copyrighted as indicated in the article. Reuse of AIP content is subject to the terms at: http://scitation.aip.org/termsconditions. Downloaded to IP: 131.215.71.79 On: Thu, 20 Mar 2014 14:54:09

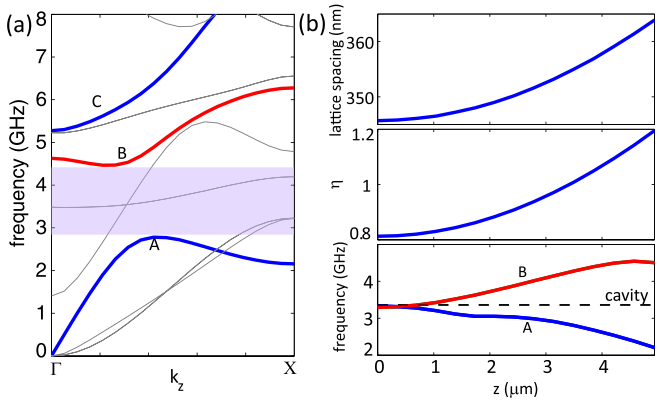

FIG. 3. (a) Phononic bands for a periodic array of holes with $a = 350$ nm. Modes on bands A, B, and C are symmetric across planes x, y, and z. Modes on the gray bands have other types of spatial symmetries. (b) (top) Hole spacing, (middle) hole aspect ratio factor $\eta(z)$, and (bottom) A band maximum (blue) and B band minimum (red) frequencies as functions of distance z along the cavity. Bottom panel, dashed line: fundamental breathing mode frequency.

contract symmetrically. We found that the quadratic lattice constant modulation was insufficient to produce a well-confined mechanical mode, yielding only a relatively small shift of the mechanical bands. To overcome this, we allowed the minor and major radii of the elliptical holes to vary along the cavity as $(w_z(z), w_x(z)) = (w_{z,0}/\eta(z), w_{x,0} \cdot \eta(z))$, with quadratic $\eta(z)$ (Fig. 3(b), middle). This causes the strong modulation of the edges of bands A and B, see in Fig. 3(b), bottom, so allowed frequencies at $z = 0$ (cavity center) fall within the phononic bandgap of the outer regions ($z > 5\,\mu$m). The breathing mode frequency is indicated with a dashed line in Fig. 3(c). The $\eta(z)$ profile of Fig. 3(b) was obtained with a nonlinear optimization routine that sought to maximize the optomechanical coupling rate g_0 while keeping the optical quality factor above 10^6. The hole aspect ratio modulation does cause the photonic band edges to shift as shown in Fig. 2(c). High Q_o optical modes can still be found, albeit at frequencies shifted from the original. The optimized OMC design yielded $g_0/2\pi = 133.6$ kHz ($L_{OM} = 5.1\,\mu$m) for an optical mode at $\lambda = 966$ nm.

Devices were fabricated on stoichiometric Si_3N_4 (tensile stress of ≈800 MPa) with electron-beam lithography and reactive ion etching with a CHF_3:O_2:Ar mixture. Suspended nanobeams were obtained by etching the underlying Si substrate with a Potassium Hydroxide (KOH) solution. Fabricated devices were initially characterized with optical transmission spectroscopy (Fig. 4(a)). Light from a tunable external cavity diode laser was coupled to the devices using an optical fiber taper waveguide (FTW), as in Fig. 4(a). A polarization controller before the FTW allowed coupling to TE cavity modes to be maximized. The laser wavelength was swept, and the signal transmitted through the FTW was detected and recorded, revealing optical resonances in the 980 nm band with $10^4 < Q < 1.3 \times 10^5$ (Fig. 4(c)). Mechanical modes coupled to a particular optical resonance were measured at low optical power by tuning the laser wavelength to the shoulder of the optical mode. Resonance fluctuations induced by thermal-noise-driven mechanical motion were converted to an intensity modulation of the transmitted optical signal. The transmitted optical signal was detected with an avalanche photodiode (APD), and the electrical signal was resolved in a spectrum analyzer. A typical spectrum showing a peak due to the fundamental breathing mechanical mode at ≈3.8 GHz is shown in Fig. 4(d). With a quality factor $Q_m \approx 3000$ at atmosphere, the frequency-Q_m product is $\approx 12 \times 10^{12}$, twice that observed in vacuum and at 8 K in Ref. 14. The high mechanical frequency ensures that the system is in the resolved-sideband regime ($\omega_m/\kappa \approx 1.6$).

The typical sideband resolution achieved was sufficient for the observation of optomechanical EIT at room temperature and atmospheric pressure. This effect corresponds to the creation of a narrow transparency window in the optical transmission spectrum (and, correspondingly, a dip in reflection) by pumping the optical cavity at a red-detuned frequency from the cavity center. It is a macroscopic manifestation of the coherent interaction between cavity

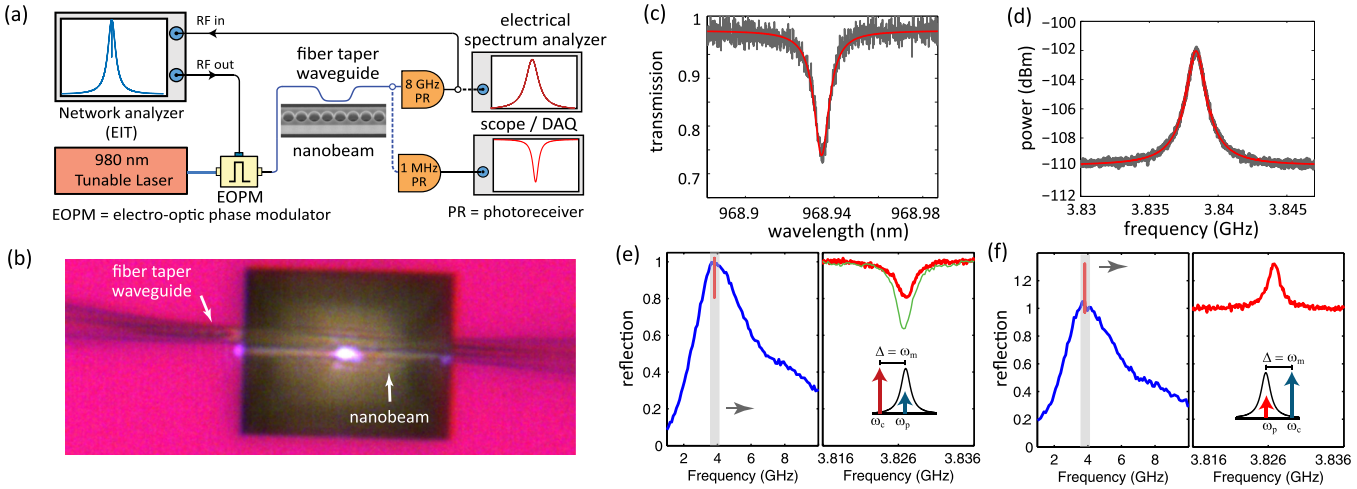

FIG. 4. Experimental data. (a) Setup for optical and mechanical mode characterization. (b) Microscope image of fiber taper waveguide coupled to nanobeam cavity. DAQ = data acquisition. (c) Optical transmission spectrum showing resonance dip with $Q_o = 116 \times 10^3 \pm 5 \times 10^3$. (d) Optical signal RF spectrum showing peak due to thermal motion of the fundamental breathing mechanical mode, with $Q_m = 3152 \pm 30$. (e) Optical reflection spectrum for red-detuned pump $\approx\omega_m$ from the resonance center (see inset). Left panel: broad range spectrum; right panel: blow-up of reflection spectrum around the mechanical frequency, showing the EIT dip for CW pump. Green line: same, pulsed pump. (f) Same as (c), for blue-detuned pump. Left panel: reflection peak consistent with electromagnetically induced absorption. Errors in Q_o and Q_m are 95% fit intervals, corresponding to 2 standard deviations.

This article is copyrighted as indicated in the article. Reuse of AIP content is subject to the terms at: http://scitation.aip.org/termsconditions. Downloaded to IP: 131.215.71.79 On: Thu, 20 Mar 2014 14:54:09

photons and phonons as it stems from the destructive interference between an incident probe signal and anti-Stokes pump photons scattered by the mechanical resonance. Optomechanical EIT has been observed in many systems, including silica microtoroids[15] and microspheres,[16] Si OMCs,[1] and Si_3N_4 microdisks,[14] although these previous demonstrations were typically done in vacuum (and in many cases, at cryogenic temperatures).

To measure this effect, an electro-optic phase modulator was used to produce sidebands on a continuous wave (CW) control beam. With the control field fixed at a frequency ω_c, Δ away from the optical resonance at ω_o, the modulation frequency was varied over the range 100 MHz–20 GHz, which allowed the sidebands to scan over the entire optical resonance. As detailed in Ref. 9, detection of the modulated signal with the 8 GHz photoreceiver and demodulation in a vector network analyzer produced the cavity reflectivity spectra in Fig. 4(e). The left panel of Fig. 4(e) shows the reflection spectrum over a broad frequency range, indicating an optical cavity FWHM of ≈4.4 GHz. The red portion of the curve is the superimposed spectrum shown on the right panel, where the reflectivity dip due to EIT is clearly evident. Figure 4(f) shows the same for a blue-detuned pump. Here, optomechanical electromagnetically induced absorption (EIA) manifests itself as a peak in reflection, corresponding to constructive interference between the probe and Stokes-scattered pump photons. Assuming $\Delta \approx \omega_m$ (ω_m is the mechanical frequency), a cooperativity $C = 0.12$ was estimated via a fit to the EIT and EIA spectra.[9] From the transmission spectrum and control laser detuning Δ, we estimate an intracavity photon population of $N = (9.73 \pm 1.34) \times 10^3$, and thence, an optomechanical coupling rate $g_0/2\pi = 170$ kHz ± 17 kHz,[9] higher than the theoretical $g_0/2\pi \approx 130$ kHz (uncertainties are of one standard deviation). The discrepancy is possibly due to geometrical variations between the fabricated device and the simulated model. Another possibility is the existence of a constructive elasto-optic contribution,[10] which is not included in our model.

Linear absorption in the Si_3N_4 leads to a red-shift of the optical resonance frequency (thermo-optic effect) which increases with cavity photon number and results in a bistable dynamic behavior.[17] At sufficiently high powers, the shift reaches an unstable maximum, and the cavity snaps back to its original frequency. In recent work with Si_3N_4 microdisks,[14] these issues were mitigated by cryogenic cooling and actively locking the pump laser to the cavity. The achieved C was nevertheless limited to 0.5 in spite of the larger intracavity photon number ($\approx 6 \times 10^4$) and higher optical and mechanical quality factors ($Q_o = 5 \times 10^5$, $Q_m = 10^4$) than here. This was due to the optomechanical coupling rate, $g_0/2\pi \approx 10$ kHz, >10× lower than in the Si_3N_4 OMC. This comparison indicates that high g_0 is of practical importance, offsetting the effects of limited sideband resolution, mechanical quality factor, and thermo-optic dispersion. Here, achieving significantly higher N and C under CW pumping was limited by thermo-optic cavity dispersion and instability. To mitigate this, we performed EIT measurements with a pulsed pump[9] and were able to reach a maximum population of $N \approx 3 \times 10^4$ (3× that for CW). A maximum $C = 0.264 \pm 0.01$ was observed (green curve in Fig. 4(e)). Evidence of nonlinear absorption was also observed.[9]

In summary, we have designed a Si_3N_4-based nanobeam optomechanical crystal supporting $Q_o > 10^6$ optical resonances in the 980 nm wavelength band and breathing mechanical modes in the 4 GHz range, with relatively high optomechanical coupling rates ($g_0/2\pi = 130$ kHz). With high mechanical frequencies, nanobeam cavities with optical quality factors of $\approx 10^5$ were operated in the sideband resolved regime and were used to demonstrate electromagnetically induced transparency and absorption at room temperature and atmospheric pressure, with intracavity photon numbers on the order of 10^4. The observed mechanical frequency-Q_m product was $\approx 12 \times 10^{12}$. Moving towards $C \gg 1$—as necessary, e.g., quantum level photon-phonon translation (Ref. 4)—our results suggest that strategies for producing enhanced zero-point optomechanical coupling rates such as slot-mode type OMCs[18] can be advantageous for Si_3N_4 devices, which, unlike silicon devices, are able to support large intracavity photon numbers ($\approx 10^4$) before starting to show signs of nonlinear absorption. Other wide bandgap materials, including AlN (Ref. 19) and GaP (Ref. 20) (which has refractive index ≈3) are promising candidates as well.

We thank Vladimir Aksyuk and Oskar Painter for helpful discussions. This work was partially supported by the DARPA MESO program. S.A. acknowledges support under the Cooperative Research Agreement between the University of Maryland and NIST-CNST (Award No. 70NANB10H193). Y. L. acknowledges support under the NIST-ARRA Measurement Science and Engineering Fellowship Program Grant No. 70NANB10H026 through the University of Maryland.

[1]A. H. Safavi-Naeini, T. P. M. Alegre, J. Chan, M. Eichenfield, M. Winger, Q. Lin, J. T. Hill, D. E. Chang, and O. Painter, Nature (London) **472**, 69 (2011).
[2]J. Chan, T. P. M. Alegre, A. H. Safavi-Naeini, J. T. Hill, A. Krause, S. Gröblacher, M. Aspelmeyer, and O. Painter, Nature (London) **478**, 89 (2011).
[3]T. J. Kippenberg and K. J. Vahala, Science **321**, 1172 (2008).
[4]A. H. Safavi-Naeini and O. Painter, New J. Phys. **13**, 013017 (2011).
[5]E. Verhagen, S. Deléglise, S. Weis, A. Schliesser, and T. J. Kippenberg, Nature **482**, 63 (2012).
[6]J. D. Teufel, D. Li, M. S. Allman, K. Cicak, A. J. Sirois, J. D. Whittaker, and R. W. Simmonds, Nature **471**, 204 (2011).
[7]S. S. Verbridge, H. G. Craighead, and J. M. Parpia, Appl. Phys. Lett. **92**, 013112 (2008).
[8]J. F. Bauters, M. J. R. Heck, D. John, D. Dai, M.-C. Tien, J. S. Barton, A. Leinse, R. G. Heideman, D. J. Blumenthal, and J. E. Bowers, Opt. Express **19**, 3163 (2011).
[9]See supplementary material at http://dx.doi.org/10.1063/1.4858975 for details on simulations, fabrication, experimental setups, and data analysis.
[10]J. Chan, A. H. Safavi-Naeini, J. T. Hill, S. Meenehan, and O. Painter, Appl. Phys. Lett. **101**, 081115 (2012).
[11]P. T. Rakich, C. Reinke, R. Camacho, P. Davids, and Z. Wang, Phys. Rev. X **2**, 011008 (2012).
[12]Q. Quan and M. Loncar, Opt. Express **19**, 18529 (2011).
[13]K. Srinivasan and O. Painter, Opt. Express **10**, 670 (2002).
[14]Y. Liu, M. Davanço, V. Aksyuk, and K. Srinivasan, Phys. Rev. Lett. **110**, 223603 (2013).
[15]S. Weis, R. Rivière, S. Deléglise, E. Gavartin, O. Arcizet, A. Schliesser, and T. J. Kippenberg, Science **330**, 1520 (2010).
[16]C. Dong, V. Fiore, M. Kuzyk, and H. Wang, Science **338**, 1609 (2012).
[17]P. Barclay, K. Srinivasan, and O. Painter, Opt. Express **13**, 801 (2005).
[18]M. Davanço, J. Chan, A. H. Safavi-Naeini, O. Painter, and K. Srinivasan, Opt. Express **20**, 24394 (2012).
[19]L. Fan, X. Sun, C. Xiong, C. Schuck, and H. X. Tang, Appl. Phys. Lett. **102**, 153507 (2013).
[20]M. Mitchell, A. C. Hryciw, and P. E. Barclay, e-print arXiv:1309.6300 (2013).

This article is copyrighted as indicated in the article. Reuse of AIP content is subject to the terms at: http://scitation.aip.org/termsconditions. Downloaded to IP: 131.215.71.79 On: Thu, 20 Mar 2014 14:54:09